



A00-16398

**AIAA 2000-0519**

**Boundary Layer Separation Control with  
Directed Synthetic Jets**

D. C. McCormick

United Technologies Research Center  
East Hartford, CT

**38th Aerospace Sciences  
Meeting & Exhibit**

**10-13 January 2000 / Reno, Nevada**

For permission to copy or to republish, contact the American Institute of Aeronautics and Astronautics,  
1801 Alexander Bell Drive, Suite 500, Reston, VA, 20191-4344.

## BOUNDARY LAYER SEPARATION CONTROL WITH DIRECTED SYNTHETIC JETS

D. C. McCormick\*

United Technologies Research Center  
East Hartford, CT 06108**ABSTRACT**

A new concept for boundary layer separation control has been developed that is a derivative of the synthetic jet concept (being used primarily for virtual shape control) which converts acoustic oscillations into mean fluid motions. The new concept, the so-called "directed synthetic jet", has an acoustically excited neck like the synthetic jet, however the neck is curved in the downstream tangential direction. In this manner, the boundary layer flowing over the neck or slot is energized via suction removal of the approaching low momentum fluid on the in-stroke and tangential blowing of high momentum on the out-stroke, thereby making it in the time average more resistant to separation. The concept has been demonstrated to be energy efficient comparing input power to system benefit, yielding a net power gain and also potent enough to completely suppress boundary layer separation. An electro-acoustic model is presented which describes the actuator characteristics and enables realistic application analysis.

**NOMENCLATURE**

$A_N$	neck or slot area ( $m^2$ )	$h$	width of neck, or slot (m)
BL	voice coil force constant = magnetic flux x voice coil length (N/amp)	$K_D$	neck jet dump loss coefficient
$c$	speed of sound (m/s) or airfoil chord (m)	$L_N$	effective acoustic length of neck or slot (m)
$C_L$	lift coefficient = Lift per unit span / ( $.5\rho U_{REF}^2 c$ )	$M_D$	moving speaker mass (kg)
$C_p$	static pressure coefficient = $(P - P_{REF}) / Q_{REF}$	$M_N$	acoustic mass in neck, or slot = $\rho L_N / A_N$ ( $kg/m^4$ )
$C_v$	acoustic compliance = $V / (\rho c^2)$ ( $m^5/N$ )	$M_{AT}$	total speaker mass including air mass in acoustic terms = $M_D / S_D^2 + \text{air mass}$ ( $kg/m^4$ )
$C_\mu$	momentum coefficient = $\rho h u_N^2 / (\rho x_{REF} U_{REF}^2)$	$R_e$	voice coil resistance (ohms)
$f$	frequency (Hz)	$R_{AS}$	speaker mechanical resistance in acoustic terms = $R_s / S_D^2$ ( $N-s/m^5$ )
$F^+$	nondimensional forcing frequency = $f x_{REF} / U_{REF}$	$R_{AT}$	total speaker resistance = $R_{AS} + BL^2 / R_e$ ( $N-s/m^5$ )
		$R_N$	neck acoustic resistance = $0.5 K_D \rho u_N / A_N + \text{viscous neck loss} + \text{acoustic radiation loss}$ ( $N-s/m^5$ )
		$R_s$	speaker mechanical resistance ( $N-s/m$ )
		$S_D$	effective area of speaker diaphragm ( $m^2$ )
		$u_N$	amplitude of neck or slot oscillation (m/s)
		$U_{REF}$	freestream, reference velocity (m/s)
		$V$	volume of cavity ( $m^3$ )
		$V_{SPK}$	voltage across voice coil terminals (volts)
		$x_{REF}$	characteristic length of uncontrolled separation (e.g., for airfoil with leading edge separation, $x_{REF}$ = chord) (m)
		$\delta$	boundary layer thickness at 0.99 of freestream velocity (mm)
		$\alpha$	angle of attack (deg)

\*Senior Member, Senior Research Engineer  
Copyright© 1999 by United Technologies Research Center. Published by the American Institute of Aeronautics and Astronautics, Inc. with permission.

## INTRODUCTION

Boundary layer separation is a major problem which constraints/limits the design of most devices involving flow. Hence, there is a strong desire for a flow separation control technique that is not only effective at reducing or eliminating separation, but does so with small parasitic drag, energy consumption, and simple installation. Not surprisingly, there has been a tremendous amount of research and development into the control of boundary layer separation (e.g., see Refs. 1 and 2). In general terms, beyond tripping a laminar boundary layer, the approaches for separation control can be broken down into four categories: 1. tangential blowing (in all its various forms, include leading-edge slats, slotted flaps, and moving wall) to directly energize the low-momentum region at the wall, 2. wall suction to remove the low-momentum region, 3. vortex generators to enhance the convective transport of freestream momentum to the wall, and, a relatively new approach, 4. forced excitation just upstream of separation (e.g., see Refs. 3-6). The first two approaches are extremely effective at controlling separation, essentially eliminating the separation. However, this degree of control requires the complexity of internal piping from a source of pressure (or vacuum), and the parasitic cost to generate this pressure (or vacuum) source. Because of these disadvantages, suction and blowing are infrequently used (except on slotted wings achieved with variable geometry). The third approach, vortex generators, have been frequently applied due to their simplicity, however, their effectiveness is limited because of their parasitic drag (controlling extreme separation requires large vortex generators which have high parasitic drag). In addition, a development length of 10-20 boundary layer thicknesses is required between the vortex generator array and the separation which is not always available (e.g. leading-edge separation).

The fourth approach, so-called "dynamic forcing" takes advantage of the natural instability of the separated shear layer to perturbations. By periodically exciting a leading-edge airfoil separation with, for example, a small vibrating flap or an oscillating slot flow, the shear layer roll up of vorticity is modulated creating large scale, phase-locked coherent vortex structures over the downstream surface. At a preferred range of frequencies which depends on freestream velocity and airfoil chord that nominally introduces 2-3 coherent structures over the surface, a large increase in flow turning has been observed. It has been speculated that the mechanism is advancement of the shear layer reattachment via the convection of freestream

momentum toward the surface by the large-scale structures.

A relatively new flow control device that has been demonstrated in computation and laboratory tests for virtual shape control is the so-called "synthetic jet". For example, applications are given by Glezer et al.<sup>7-9</sup> for thrust vectoring, bluff body and lift control and Hassan<sup>10</sup> for lift control. The synthetic jet consists of an orifice (or neck) driven by an acoustic source in a cavity (see Fig. 1). At sufficiently high levels of excitation by the acoustic source, a mean stream of flow has been observed to emanate from the neck. Because there is no mass added to the system, the mean streamlines must form a closed recirculation, as shown Fig. 1. This phenomena of "acoustic jet streaming" by an orifice under high acoustic excitation has been well known for many years. Figure 2 is from a 1953 publication<sup>11</sup> which shows the four regimes of circulation and turbulence around an acoustically excited orifice plate in terms of acoustic neck velocity (amplitude) versus frequency. The dashed line corresponds to the where the amplitude of the particle displacement in the orifice equals the orifice length. At low levels of excitation in region 1 (well below the dashed line), fluid particles move in and out of the orifice a small amount without mixing with the particles outside the orifice. A small amount of acoustic energy is lost to the surroundings via acoustic radiation (like a moving diaphragm in a wall). Near and above the dashed line in region 3, significant turbulence is generated around the orifice, hence some acoustic energy is converted into mean fluid motion. At higher levels of excitation in region 4, the fluid particle displacement extends well outside the orifice providing sufficient time for the particles to roll up into ring vorticities (for a circular aperture), separate from the orifice region, and convect away under vortex induced motions, as shown in Fig. 1, forming the mean stream of flow, or synthetic jet.

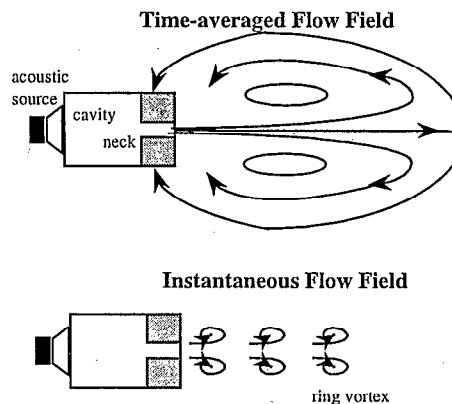


Fig. 1. Synthetic Jet Concept

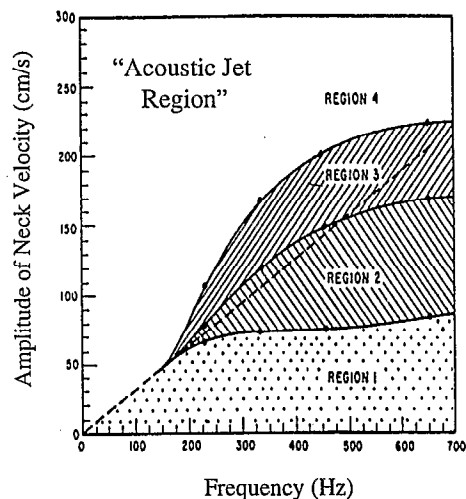


Fig. 2. Acoustic Streaming Criterion (Ingard, Ref. 11)

The main criterion to whether the acoustic oscillation in the neck couples to mean flow is related strongly to the residence time that the neck fluid particles are exposed to shear outside of the orifice. Relatively long times allow the Kelvin-Helmholtz instability develop and generate well defined vortex structures that break away for the orifice and propagate under induced-vortex motion, creating an acoustic stream.

The recent PIV velocity field measurements by Rediniotis et al.,<sup>12</sup> showed a significant difference between 10 Hz and 100 Hz for the same velocity amplitude oscillation which they attributed to a Strouhal number effect. At 10 Hz, significant vortex rollup was observed versus 100 Hz which showed no vortex rollup. It is believed that the criterion suggested by Ingard is useful in understanding their results. For the configuration tested ( $t = 6$  mm), the critical neck velocity (i.e., where amplitude of particle displacement equal length of orifice) is calculated to be 0.38 m/s which is comparable to the reported excitation level of 0.1 m/s. Considering how the regions in Fig. 2 collapse at very low frequency, is it reasonable to assumed acoustic streaming will occur, consistent with the results of Ref. 4. At 100 Hz, the critical neck velocity is 3.8 m/s, or nearly 40 times the applied level. Therefore, it is reasonable to assume (based on Fig. 2) that acoustic streaming will not occur, again consistent with the results of Ref. 4.

Though this acoustic jet streaming phenomena has been known for years, Glezer et al.<sup>7</sup> were the first believed to use it for flow control. Taking advantage of the closed recirculation zone, Glezer has used synthetic jets, for example as virtual curved surfaces, that when

placed by a jet, cause the jet to turn or vector dramatically (by a Coanda effect on the virtual surface).

The device described herein is a derivative of the synthetic jet which is applied to control boundary layer separation. The new concept, which we have named "directed synthetic jet" or DSJ, has been demonstrated to be extremely effective at controlling separation. In comparison with steady suction or blowing, the DSJ has less complexity, and probably much less parasitic energy cost (note that, such comparisons for system efficiency are highly system dependent, based on available pressure, vacuum and electrical sources).

### DSJ CONCEPT

The new DSJ concept is shown in Fig. 3, where the synthetic jet is embedded in the wall of a boundary layer for which separation control is desired. On the in-stroke of the neck velocity, vertical momentum is imparted to the flow causing the neck to preferentially ingest approaching low axial momentum of the incoming boundary layer (without external flow, the in-stroke would pull in flow from all directions). On the out-stroke due to the curved neck, the fluid particles are re-accelerated and injected with positive axial momentum into wall region of the boundary layer. Hence, both the in-stroke and out-stroke of the cycle increase the ability of the boundary layer to resist separation. In the time-averaged sense, the DSJ provides a step change in the shape factor of the boundary layer.

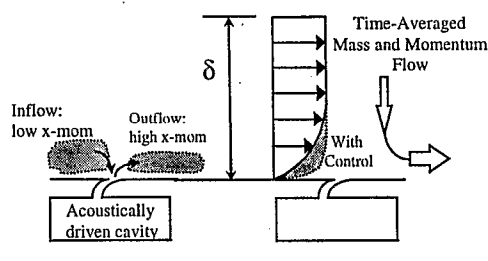


Fig. 3. Directed Synthetic Jet Concept

It is reasonable to assume that a similar acoustic streaming criterion (Fig. 2) applies to the DSJ such that a large displacement of fluid particles in the neck (which are most readily achieved at low frequencies) is required to couple the acoustic energy into the mean flow, thereby energizing the boundary layer. However, due to the convection effect of the external flow, the formation of well vortical structures (required under quiescent conditions) are not necessary for the DSJ to couple the acoustic oscillation to mean flow. It is intuitively expected the critical neck velocity will be relaxed with the addition of external flow.

Figures 4 and 5 shows the results of CFD analysis of a laminar flat plate boundary layer interacting with DSJ in terms of distance from the wall versus streamwise velocity. The slot width in this calculation is  $h = 6.4$  mm, the amplitude of the slot velocity is 10 m/s, and the freestream velocity is 20 m/s. In Fig. 4, the instantaneous profiles downstream of the slot (11 mm) at the peak of the in-stroke and peak of the out-stroke are shown versus the baseline, no forcing case (solid line). The in-stroke profile illustrates the removal of the low-momentum fluid (as well as a freestream velocity decrease by diffusion due to the decrease in boundary layer blockage). The out-stroke profile illustrates the high-momentum injection (as well as freestream velocity increase due to the increased blockage from the flow addition). The time-averaged controlled boundary versus the baseline profile is given in Fig. 5 which shows the energization effect of the DSJ. In addition, there is a net diffusion of the freestream flow indicating the DSJ has a boundary layer thinning effect. As would be expected, the CFD results also display in the vicinity of the DSJ a negative vertical velocity component toward the surface. Hence, an additional benefit of the DSJ is to drive freestream momentum closer to the surface.

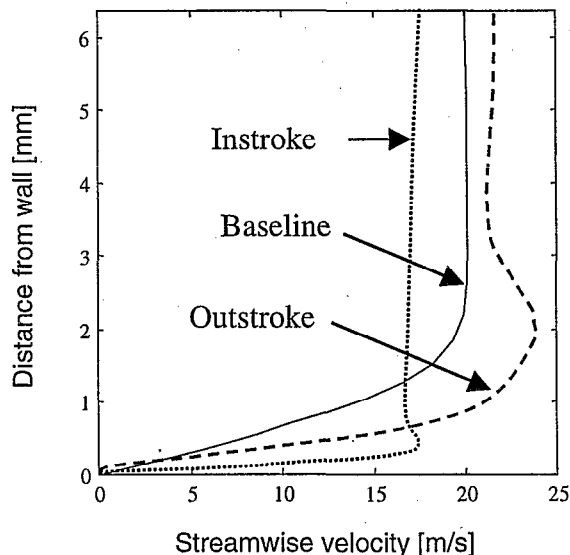


Fig. 4. Flat Plate, Instantaneous Velocity Profiles With and Without Control

Admittedly, the DSJ device illustrated in Fig. 3 has similarities to that of previous investigations of dynamic separation control.<sup>5</sup> However, the application of the device and the design methodology are different (i.e., separation suppression through energization of the boundary layer). This feature also makes it possible that this concept can be effectively distributed (possibly

via microfabrication) such that when the boundary layer begins to weaken and approach separation, another DSJ can be applied to re-energize the boundary layer, as suggested in Fig. 3. This is possible as long as the spacing is not so close that the high momentum injected by one DSJ is ingested by the next downstream DSJ, though this may be addressed through phasing. The idea of separation control via boundary layer energization with a curved-neck synthetic jet has been also suggested recently by Rediniotis, who attributed their control to additional mechanisms (Coanda and dynamic separation control).<sup>12</sup> This work was limited in the very low Reynolds number, laminar flow in water and did not completely suppress the separation, in contrast with the present investigation.

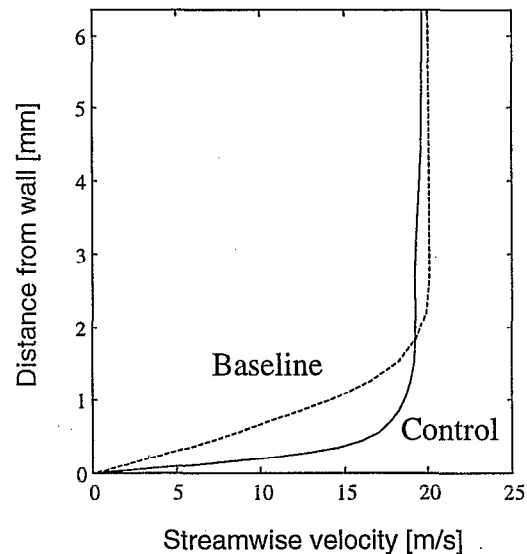


Fig. 5. Flat Plate, Averaged Velocity Profiles With and Without Control

As discussed below, DSJ concept generally requires higher levels of  $C_\mu$  (2-3x) than that of dynamic separation control, however, the advantage is in the robustness and the ability to optimize the system efficiency at a single frequency through actuator resonance. An additional advantage of the embodiment in Fig 3, is if insufficient forcing levels are achieved, it can act as an effective dynamic separation control actuator (as has been demonstrated several times by other investigators).

#### DIFFUSER DEMONSTRATION

The DSJ concept has been demonstrated in a 2-D diffuser wind tunnel shown in Fig. 6. The DSJ is located at the corner at the diffuser inlet. The boundary layer at the inlet is turbulent, approximately  $\delta = 6.4$

mm thick. The DSJ is driven by a JBL 2118 8 inch speaker and the slot is nominally 6.4 mm wide and curved with nominally a 6.4 mm radius. Based on a Kline chart,<sup>13</sup> this diffuser is quite aggressive (at edge of the “fully developed 2-D stall” regime). Figure 7 gives the pressure coefficient,  $C_p$ , based on reference conditions located 23 cm upstream of the diffuser inlet, versus axial location,  $x$ , for a range of speaker power at 50 Hz. Without forcing, there is no pressure recovery, actually losing pressure. This, however, is caused by the discontinuity introduced by the slot. A more appropriate baseline is the pressure recovered by a smooth corner which was found to have a recovery of  $C_{PEXIT} = 0.1$ . Applying forcing clearly improves the pressure recovery monotonically with speaker power up to 5 Watts (based on the nominal DC resistance, 8 ohms, and terminal voltage of the voice coil) where the improvement saturates at a high recovery value of  $C_{PEXIT} = 0.45$  (or  $\sim 0.55$  if inlet reference conditions are used). The saturation in performance is due to the upper wall boundary layer separating, hence, controlling both walls would allow even greater improvement. Also shown in the figure is the no-control, optimal-diffuser case (wall angle of  $\theta = 13^\circ$ ), which allows a pressure recovery of  $C_{PEXIT} = 0.27$ . Hence, the controlled recovery significantly outperforms the recovery of the optimal diffuser angle. This contrasts with a previous (unpublished) work which used low-profile vortex generators to control separation in this diffuser wind tunnel. The vortex generator (VG) control at high wall angles was found to improve on the no-VG performance substantially, but never to the point where it was better than the no control, optimal-wall angle case. This is caused by the VG's limited effectiveness relative to its parasitic drag.

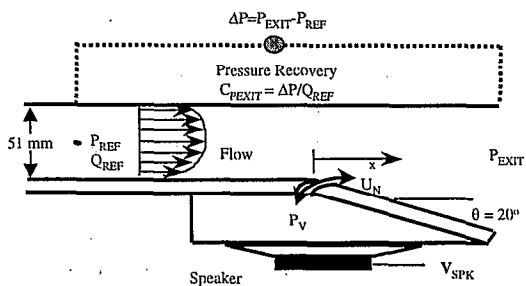


Fig. 6. Diffuser Experimental Arrangement

To quantify the level of neck velocity forcing, phase-locked hot wire anemometer surveys were taken across the slot and spatially integrated to determine the area-averaged velocity amplitude. The forcing level is documented in terms of the momentum coefficient typically defined as,  $C_\mu = \rho u_N^2 / (\rho x_{REF} U_{REF}^2)$ , which is a ratio of neck momentum-to-freestream momentum

(actually twice the RMS value). The corresponding  $C_\mu$  levels are listed in Fig. 7, using a reference length of  $x_{REF} = 0.2$  m (length of the diffuser wall). A value of  $C_\mu = 0.006$  is required to saturate the performance. In terms of the typical normalized frequency,  $F^* = f x_{REF} / U_{REF} = 0.5$ .

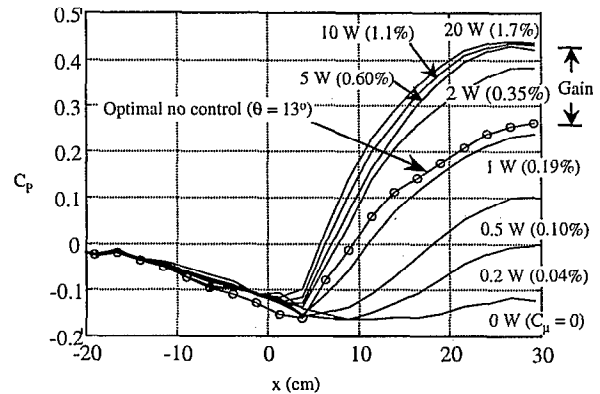


Fig. 7. Static Pressure Distribution Versus Forcing Level In Diffuser

In terms of efficiency, a very conservative baseline for comparison is the optimal pressure recovery without flow control achieved with a rounded corner (no slot) and reduced diffuser angle of  $\theta = 13^\circ$ . Based on the increased pressure rise over this case (labeled as “Gain” in Fig. 7), the flow power (total pressure times flow rate) is reduced at a given flow rate. Converting this reduction in flow power to the electrical power needed to generate it (typical motor efficiency of 50% and centrifugal fan efficiency of 50%) and comparing it to the actual speaker power (measured with a power meter) showed that there was a 16:1 return on the input electrical power to the speaker. Based on the hot wire data, it was found that the efficiency of converting speaker input electric power into flow power in the neck was only about 15% efficient. This low efficiency is partly due to the fairly-well damped speaker that was used (quality factor = 2.4). Recent improvements in the speaker design have increased this efficiency (input speaker power to slot flow power) to 40%. Hence, it is reasonable to expect with an optimized speaker-driven DSJ, a 45:1 return on input electrical power is very achievable.

The frequency and amplitude dependence of the overall pressure recovery,  $C_{PEXIT}$ , is shown in Fig. 8. Below 5 W, the performance is best around 100 Hz, drops off rapidly above 350 Hz, and approaches zero above 400 Hz. As discussed below the actuator resonance is at 50 Hz, hence, the preference for 100 Hz ( $F^* = 1$ ) is presumed to be a dynamic effect. Above 3 W, the frequency dependence flattens substantially

indicating the effect of the separation suppression. Tests were also performed at 112 f/s, which indicated the flattening effect to occur at relatively lower power level. This is reasonable to expect since there is better alignment at the higher speed between the actuator and diffuser modes. Note that at 5 Watts, the performance becomes somewhat erratic (150-200 Hz). This was caused by detrimental effects of the induced separation on the (uncontrolled) upper wall of this particular diffuser, and hence should be ignored.

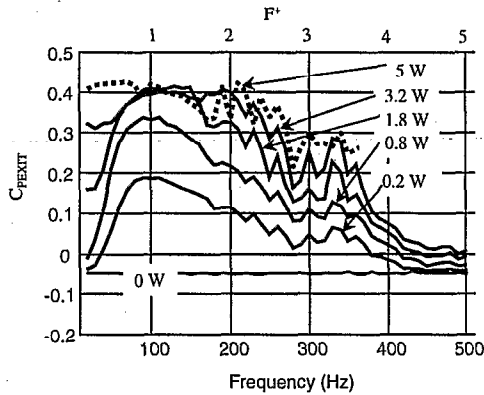


Fig. 8. Frequency Dependence of Diffuser Pressure Recovery

### ACTUATOR MODEL

In order to understand the frequency dependence observed in Fig. 8, an acoustic model of the speaker, cavity, and neck (slot) of the DSJ was developed to relate speaker input,  $V_{SPK}$ , to neck acoustic velocity,  $U_N = u_N A_N$ . Such a model not only helps understand the observed frequency response of a given DSJ arrangement, but can be used to optimize practical applications of the technology in order to minimize power consumption by the device.

Figure 9 shows a schematic of the physical arrangement and Figure 10 gives the equivalent electro-acoustic circuit for the DSJ. The modeling approach is similar to that described in Ref. 14.  $M_N$  is the inductive mass of the neck =  $\rho L_N / A_N$ ,  $L_N$  is the effective length of the neck,  $A_N$  is neck area,  $R_N =$  neck resistance  $\sim 0.5K_D \rho u_N / A_N$  (i.e., jet dump loss dominated),  $K_D$  is the neck jet dump loss coefficient,  $P_V$  is the pressure in the volume,  $C_V$  is the cavity compliance =  $V / \rho c^2$ ,  $R_{AT}$  is the sum of the mechanical resistance due to the speaker suspension and the electrical resistance due to the voice coil,  $M_{AT}$  is the sum of the speaker mass and air mass moving with the speaker,  $C_{AS}$  is the compliance of the speaker suspension,  $BL$  is the product of the magnetic field flux and voice coil length,  $R_e$  is the resistance of the voice coil, and  $S_D$  is the effective speaker area. At moderate and high excitation levels the dominant loss

mechanism in the neck is jet dump loss (nonlinear) which far exceeds the neck viscous loss and acoustic radiational loss. For  $K_D = 1$ , this resistance represents the conversion of acoustic neck oscillations into mean flow (desired), whereas higher values represent separation losses in the neck and effective area changes due to vena contracta effects. Due to the nonlinear resistance, the circuit was solved iteratively for a given  $V_{SPK}$  amplitude until the neck velocity converged.

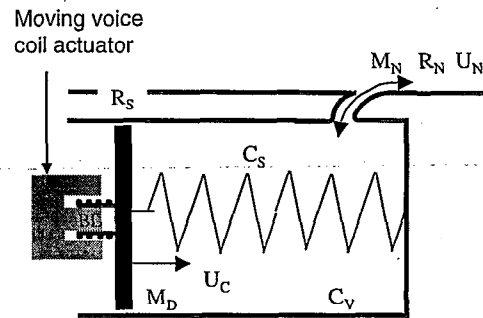


Fig. 9. Schematic of Electro-Acoustic Model of DSJ

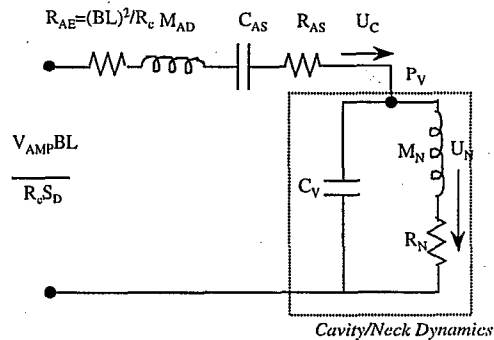


Fig. 10. Electro-Acoustic Model of DSJ

The main uncertainties in the model are the effective length ( $L_N$ ) of the neck and the jet dump loss coefficient. Variation estimates of these for high amplitude and high aspect ratio necks (i.e., slots) can be found from previous Helmholtz resonator work.<sup>11</sup> However, an easy and accurate means to determine them is to passively excite the system with an external noise source in a swept sine manner and measure the transfer function between external and cavity pressure. An electroacoustic model of this case can easily be made (similar to Fig. 10) and solved directly for this transfer function (with an actuator or a hard wall condition) in terms of the uncertain parameters which can then be adjusted to fit the experimental results. Model versus experimental transfer functions of the cavity pressure to the speaker input,  $P_V / V_{SPK}$ , for two speaker amplitudes (low - 2 Watts and high - 20 Watts) are shown in the bottom of Fig. 11. The model shows good agreement with the experimental frequency and amplitude dependence.

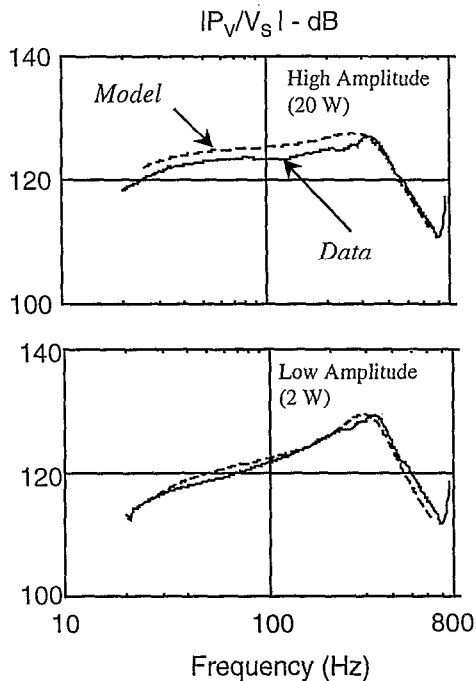


Fig. 11. Electro-Acoustic Model Versus Experiment in Terms of Cavity Pressure-Speaker Input Voltage Transfer Function.

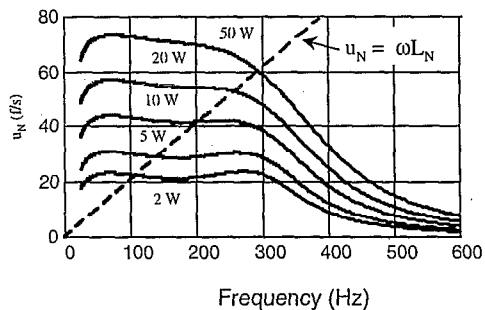


Fig. 12. Frequency Dependence of Neck Velocity with Frequency

Fig. 12 gives the predict particle neck velocity over a range of speaker power. The dashed line is Ingard's  $u_N = \omega L_N$  criterion, where particle displacement equals neck length. Recall from Fig. 2, that the coupling to achieve acoustic jet streaming is most effective above this line (at least for an isolated orifice plate). The predictions in Fig. 12 are very similar to the experimental diffuser recovery versus frequency and speaker power shown in Fig. 8 in that there is good agreement with the shape of the predicted neck velocity, in particular when the acoustic jet streaming criterion is taken into account. Like the predicted neck velocity, there is a monotonic increase in  $C_{PEXIT}$  with speaker power,  $C_{PEX}$  has two peaks around 50 and 300 Hz with the higher frequency peak being lower (due to the jet

streaming criterion), and  $C_{PEX}$  rolls off significant by 400 Hz.

### AIRFOIL DEMONSTRATION

In addition to the diffuser demonstration, the DSJ concept has been investigated for control of airfoil leading-edge separation. A 2-D airfoil section (0.44 m chord, 0.53 m span) was installed in the UTRC Acoustic Research Tunnel (ART) free jet (Fig. 13). The airfoil section is the same as that used by Lorber.<sup>15</sup> Due to the small span-to-chord ratio, side plates were installed to minimize pressure-suction side spillage and three-dimensional flow. Surface flow visualization was successfully used to design the side plates and verify the flow was parallel over the majority of the span. Due to the small wind tunnel cross section area-to-airfoil area (1.8), there was significant blockage effect which reduces the actual incidence angle. However, applying a free-jet blockage correction given in Pope<sup>10</sup> was found to be surprisingly successful at adjusting the lift/drag data and stall angle ( $\sim 14^\circ$ ) to match the data in Ref. 15 which was a full-scale, tunnel-spanning, 2-D test performed in a 2.4 m cross-sectional wind tunnel with solid walls and very small blockage. In addition, the peak lift coefficient ( $\sim 1.5$ ) and Mach number dependence over the range 0.2-0.4 ( $Re=2-4 \times 10^6$ ) was found to be in excellent agreement with Ref. 15. Hence, despite the compromised wind-tunnel/model characteristics, the test provide a cost-effective means to evaluate the DSJ concept on leading-edge separation.

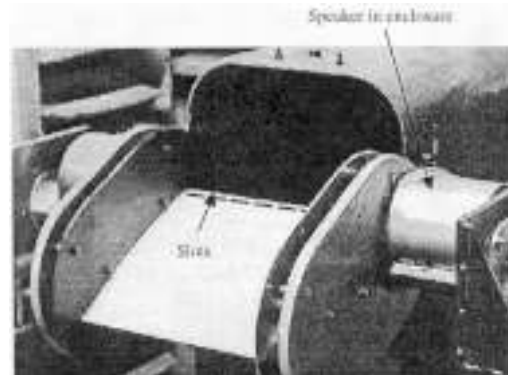


Fig. 13. Airfoil Experimental Arrangement

The DSJ was installed at a 4% chordwise location, upstream of the leading-edge separation (approximately 8% chord), by laser drilling a slot inclined approximately  $20^\circ$  from the surface over the span into the hollow leading edge. Two 5" JBL 500GTI speakers mounted outside the free jet on the ends of the airfoil were used to provide acoustic excitation of the leading-edge cavity. Due to the limited level of forcing achievable with this arrangement, most of the control



data was obtained at lower Mach numbers ( $M = 0.03-0.05$  versus  $0.2-0.4$  applied in Ref. 15) in order to increase the achievable range of  $C_{\mu}$ .

The lift results at  $M=0.05$  ( $Re = 5 \times 10^5$ ) are shown in Fig. 14 in terms of lift coefficient versus angle of attack (uncorrected for wind tunnel blockage). The baseline airfoil (no slot) performance is the thick line labeled "smooth". Due to the lower Reynolds number, the linear lift slope is somewhat decreased and the stall angle occurs earlier ( $19^\circ$  versus  $24^\circ$ ) compared with the  $M = 0.2$  ( $Re = 2 \times 10^6$ ) data from the ART, hence reducing the peak lift coefficient from 1.5 to 0.75. This Reynolds number dependence is indicative of a laminar boundary layer separation.

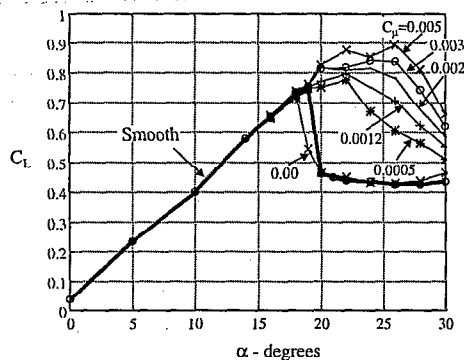


Fig. 14. Lift Performance with Various Degrees of Forcing ( $Re = 5 \times 10^5$ )

The DSJ control is shown in Fig. 14 for a range of forcing levels from  $C_{\mu} = 0 - 0.005$ . The DSJ frequency was operated at 50 Hz which was near the first resonance of the speaker system which gives an  $F^+ = 1.3$ . At  $C_{\mu} = 0$ , the presence of the slot is seen not to alter the linear lift portion, but does cause the airfoil to stall  $1^\circ$  earlier. Over the range of  $C_{\mu} = 0.0005 - 0.005$ , the post-stall lift continuously improves with increasing forcing level. At  $C_{\mu} = 0.005$ , the airfoil performance is improved by extending the stall angle by  $5-6^\circ$ , increasing maximum lift by 25%, and reducing the rate of lift loss beyond stall.

Limited data with control was taken at higher Mach and Reynolds number and frequencies other than 50 Hz. At  $M = 0.1$  ( $Re = 1 \times 10^6$ ), the linear lift slope increased and the stall angle increased by  $1^\circ$ , such that the maximum lift coefficient rose to  $C_L = 1.0$  indicative of more turbulent conditions (as would be expected at this Reynolds number). Despite these changes, when scaled to the maximum lift coefficient, the effect of forcing level was essentially the same as the lower Reynolds data (given in Fig. 14) up to the maximum achievable forcing level of  $C_{\mu} = 0.001$  at 50 Hz ( $F^+ = 0.65$ ). Hence it is concluded that the relatively low Reynolds number

of the data in Fig. 14 is applicable to moderate Reynolds number conditions that are fully turbulent. In addition, since the absolute frequency was held constant between the two Mach number cases, this result also indicates the weak sensitivity to the normalized frequency ( $F^+$ ). A more systemic investigation of frequency dependence was performed. At a post stall condition,  $M = 0.1$  ( $Re = 1 \times 10^6$ ), the forcing frequency was varied from  $F^+ = 0.25 - 3.5$  which when plotted versus the frequency dependence on  $C_{\mu}$  did not show a strong frequency preference.

Up to a forcing level of  $C_{\mu} = 0.005$ , the experimental arrangement and performance results are very consistent with that previously reported by Wagnanski et al. in terms of the benefit versus  $C_{\mu}$  level, as well as the frequency dependence being a not strong parameter over a fairly broad range of  $F^+$ .

The most interesting new result is shown in the flow visualization in Fig. 15a-d. Here, smoke is introduced just upstream of the leading edge and a vertical Laser sheet parallel to the flow is provided from a pulsed YAG laser for a post-stall angle of attack ( $\alpha = 24^\circ$ ). In order to cover a greater range of forcing levels, the wind tunnel speed was reduced to  $M=0.025$  ( $Re = 2.5 \times 10^5$ ).

Without forcing (Fig. 15a), the flow is clearly separated from the leading edge, shedding vortical structures in the shear layer as indicated in the sketch above. At  $C_{\mu} = 0.005$  (Fig. 15b), the flow has clearly turned much more and there exist three vortical structures over the airfoil chord which are locked to the forcing frequency. This is the dynamic forcing effect described extensively by Wagnanski et al., and other investigators. At a level of  $C_{\mu} = 0.01-0.015$  (Fig. 15c), the flow is completely attached with no coherent structures. This is the DSJ operating at its full potential, completely suppressing separation via boundary layer energization. At even higher levels of forcing  $C_{\mu} = 0.04-0.068$  (Fig. 15d), vortical structures are again visible, but of the opposite sense. This flow behavior is more analogous to the synthetic jet in quiescent air and is clearly above the optimal forcing level.

An upwind, time-dependent Navier-Stokes CFD analysis was performed at  $M=0.2$  ( $Re = 2 \times 10^6$ ) with steady blowing and suction, and DSJ forcing at the leading-edge slot. One results of the analysis was the relative post-stall lift enhancement benefit of the DSJ for the experimental, low Mach and Reynolds number closely matched the computation, indicating the experimental results are not limited to the low Reynolds number. Another result was the required mean blowing  $C_{\mu}$  level was 4-5 times greater than the DSJ level.

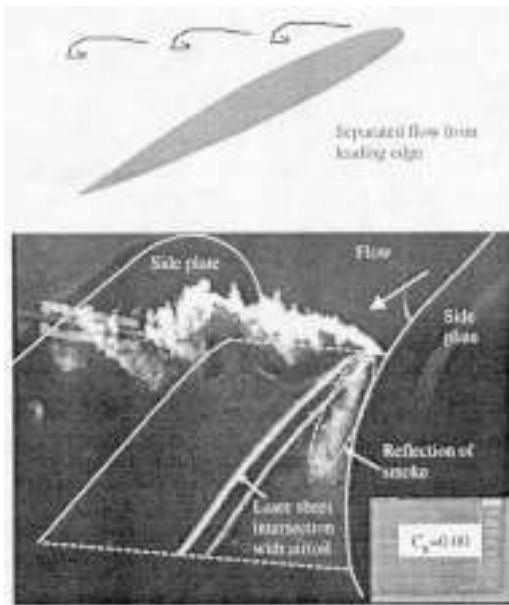


Fig. 15a. Flow visualization without forcing

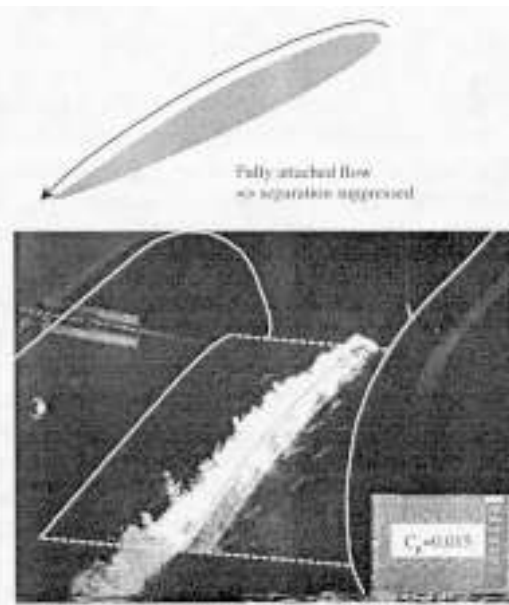


Fig. 15c. Flow visualization  $C_{\mu} = 0.015$

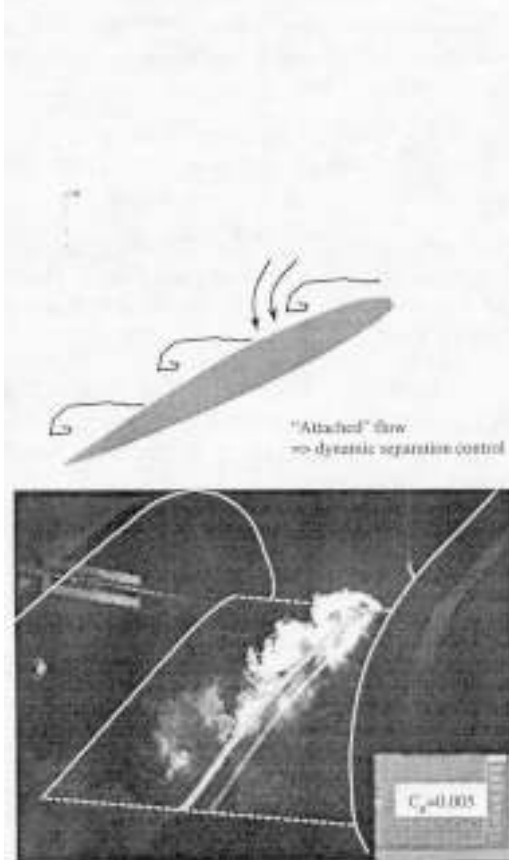


Fig. 15b. Flow visualization  $C_{\mu} = 0.005$

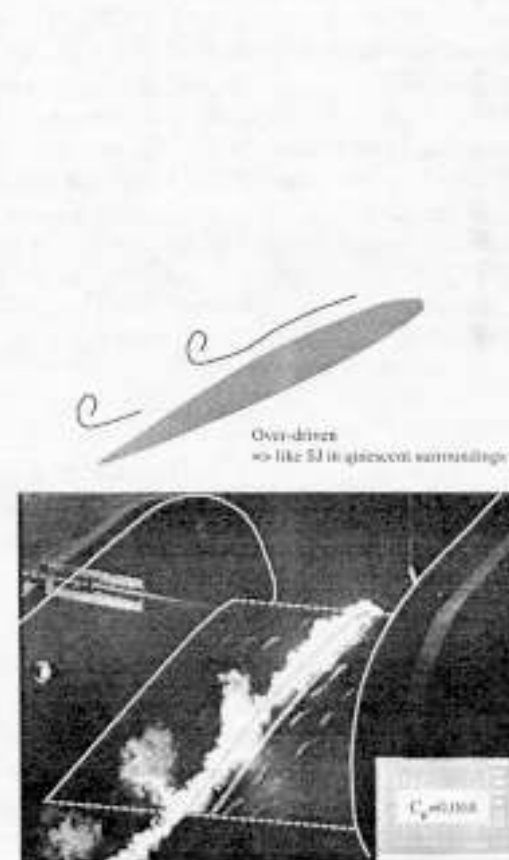


Fig. 15d. Flow visualization  $C_{\mu} = 0.068$

## CONCLUSIONS

A new concept to control boundary layer separation has been developed. The "directed synthetic jet" or DSJ, uses an acoustically-driven cavity/neck arrangement to convert acoustic energy into mean flow whereby increasing the time-averaged axial momentum of the boundary layer, making the boundary layer more resistant to separation. At sufficiently high excitation levels (well below mean blowing levels, but above dynamic separation control), the DSJ can fully suppress separation in a robust manner, insensitive to external flow parameters. Non-optimized diffuser test found a significant return on power input demonstrating its practicality. A simple electroacoustic model is developed with accurately predicts the DSJ neck velocity performance and can be used as an effective design tool for application optimization.

## ACKNOWLEDGEMENTS

Many people need to be acknowledged for this work: Dr. Daniel Gysling (now at the CiDRA corporation) as the co-developer of the DSJ concept; Drs. Douglas MacMartin, Richard Murray and Ed Greitzer for their programmatic and financial support; Drs. Dilip Prasad and Dochul Choi for the CFD analysis; Dr. Peter Lorber for his technical guidance, loan of experimental hardware for the airfoil test, and review of the manuscript; Dr. Robert Paterson for his guidance and support; and Simon Yeung and Sean Humbert for their assistance in conducting the diffuser experiments. In addition, significant laboratory support was provided by Sean Santos, Keith Post, David Terza, and Joe Poplawski.

## REFERENCES

1. Chang, P.K and Hartnett, J.P., "Control of Flow Separation: Energy Conservation, Operational Efficiency, and Safety", Series in Thermal and Fluid Engineering, Hemisphere Publishing Co., 1976.
2. Lachmann, G.V., "Boundary Layer and Flow Control", Vol. 2, Pergamon Press, Oxford, 1961.
3. Wagnanski, I, "Method and Apparatus for Delaying Separation of Flow from a Solid Surface", US Patent 5,209,438, 1993.
4. Wagnanski, I, and Seifert, A, "The Control of Separation by Periodic Oscillations", AIAA 94-2608, June 1994.
5. Seifert, A. and Pack, L.G., "Oscillatory Control of Separation at High Reynolds Numbers", AIAA 98-0214, January 1998.
6. Seifert, A., Eliahu, S., and Greenblatt, D., and Wagnanski, I., "Use of Piezoelectric Actuators for Airfoil Separation Control", AIAA Journal, Vol. 36, No. 8, August 1998, pp. 1535-1537.
7. Glezer, A., Allen, M.G. Coe, D.J., Smith, B.L., Trautman, M.A. and Wiltse, J.W., "Synthetic Jet Actuator and Application Thereof", U.S. Patent 5,758,823, June 2, 1998.
8. Amitay, M., Honohan, A., Trautmann, M., and Glezer, A., "Modification of the Aerodynamic Characteristics of Bluff Bodies Using Fluidic Actuators", AIAA 97-2004; June 1997.
9. Smith, D.R., Amitay, M., Kibens, V., Parekh, D., and Glezer, A., "Modification of Lifting Body Aerodynamics Using Synthetic Jet Actuators", AIAA 98-0209, January 1998.
10. Hassan, A, "Numerical Simulations and Potential Applications of Zero-Mass Jets for Enhanced Rotorcraft Aerodynamic Performance", AIAA 98-0211, January 1998.
11. Ingard, U, "On the Theory and Design of Acoustic Resonators", Journal of the Acoustical Society of America, Vol. 25, No. 6, November 1953.
12. Rediniotis, O.K., Ko, J., Yue, X., and Kurdila, A.J., "Synthetic Jets, Their Reduced Order Modeling and Applications to Flow Control", AIAA 99-1000, January 1999.
13. Cocanower, A.B., Kline, S.J., and Johnston, J.P., "A Unified Method for Predicting the Performance of Subsonic Diffusers of Several Geometries", Report PD-10, Thermosciences Division, Department of Mechanical Engineering, Stanford, May 1965.
14. Beranek, L.L, "Acoustics", Acoustical Society of America, Cambridge, MA, 1993.
15. Lorber, P.F. and Carta, F.O., "Airfoil Dynamic Stall at Constant Pitch Rate and High Reynolds Number", AIAA Journal of Aircraft, Vol. 25, No. 6, June 1988, pp. 548-556.
16. Rae, W.H. and Pope, A., "Low-Speed Wind Tunnel Testing", John Wiley & Sons, New York, 1984, p. 361.